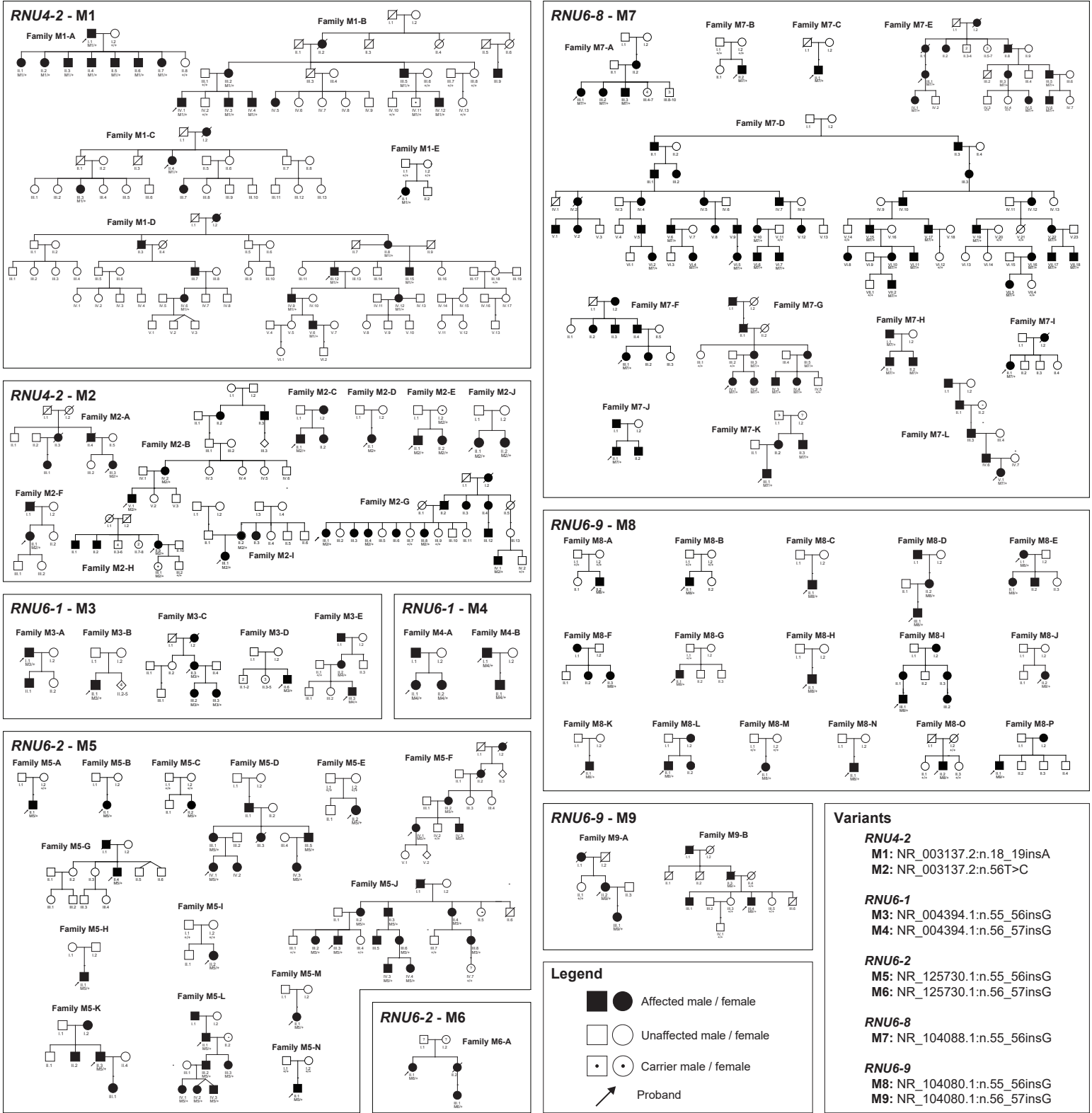
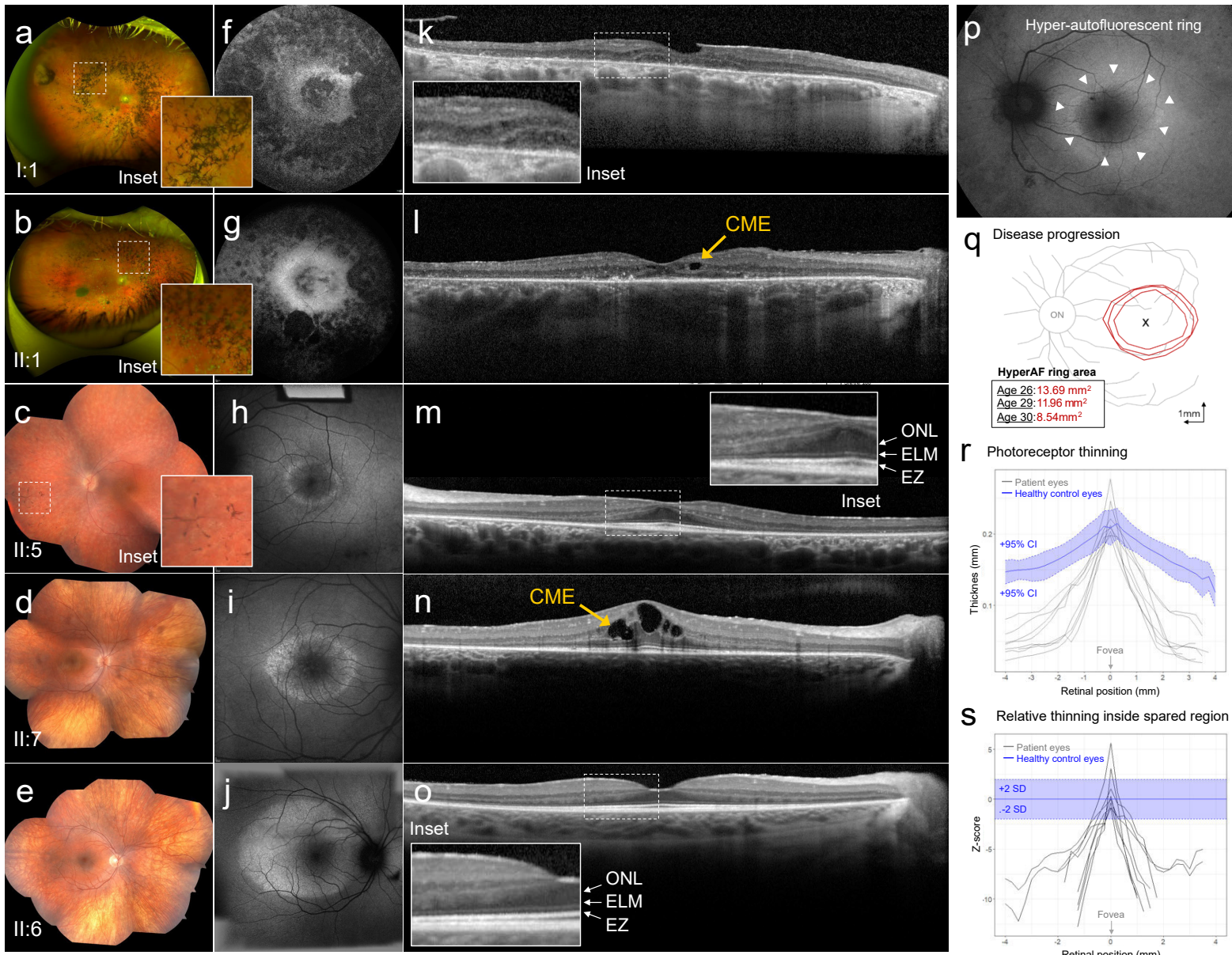


De novo and inherited dominant variants in U4 and U6 snRNA genes cause retinitis pigmentosa

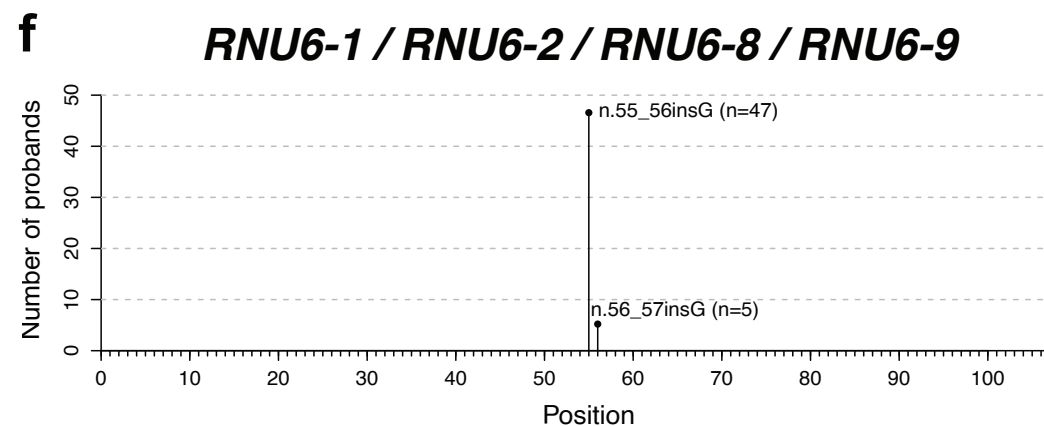
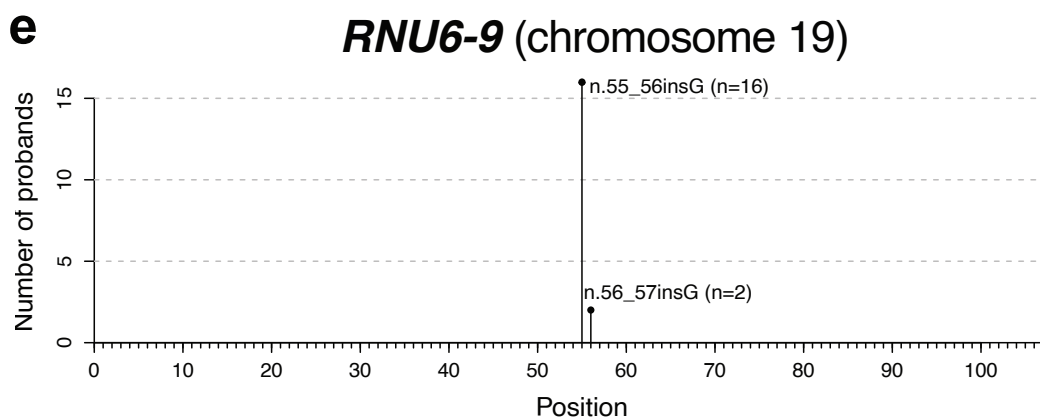
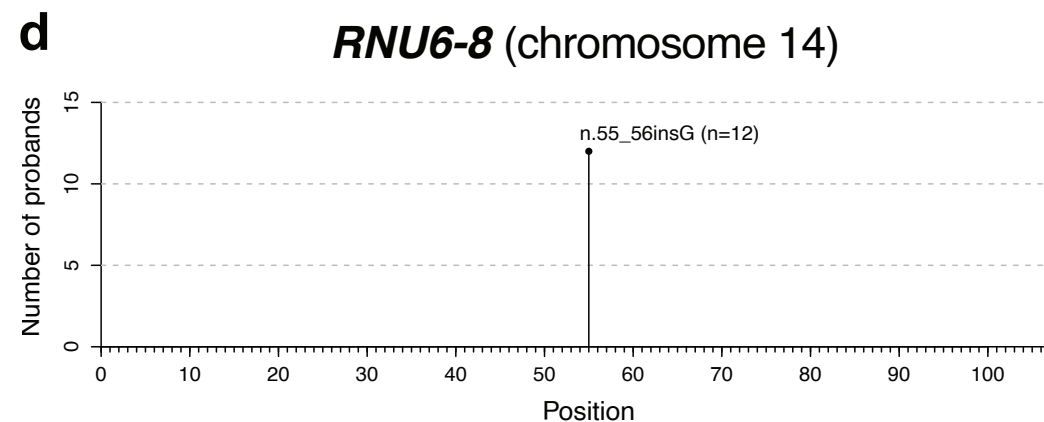
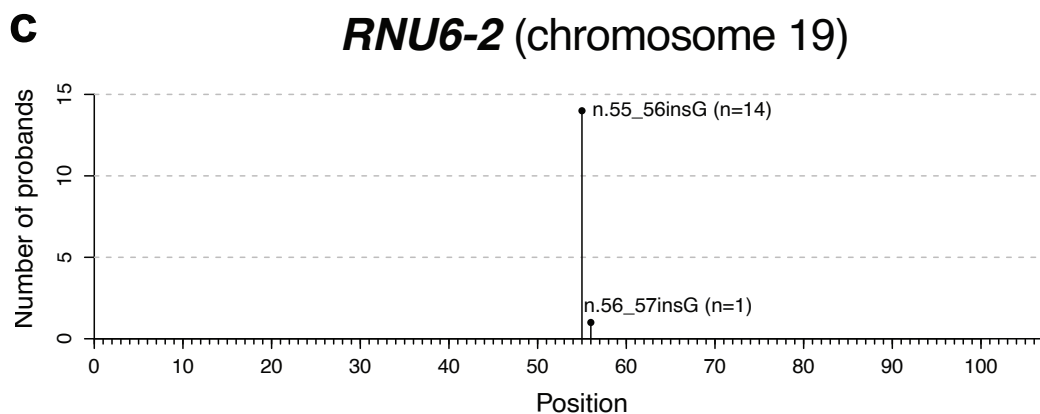
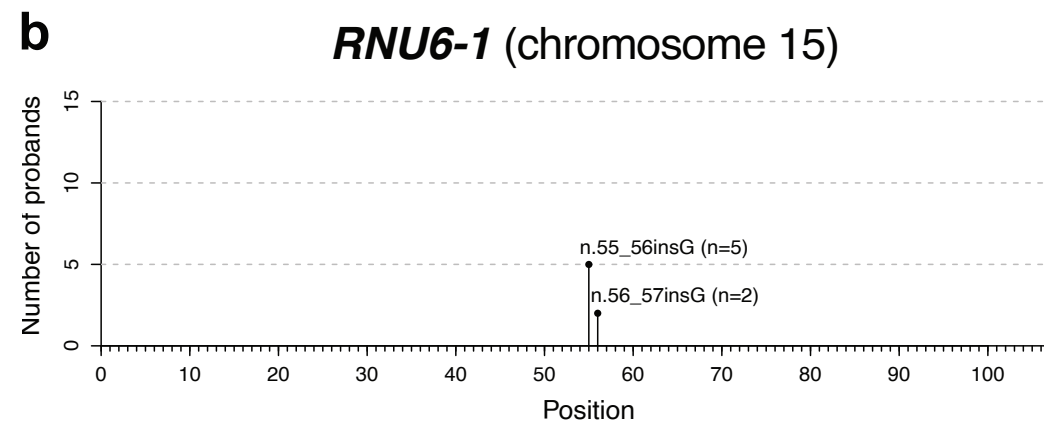
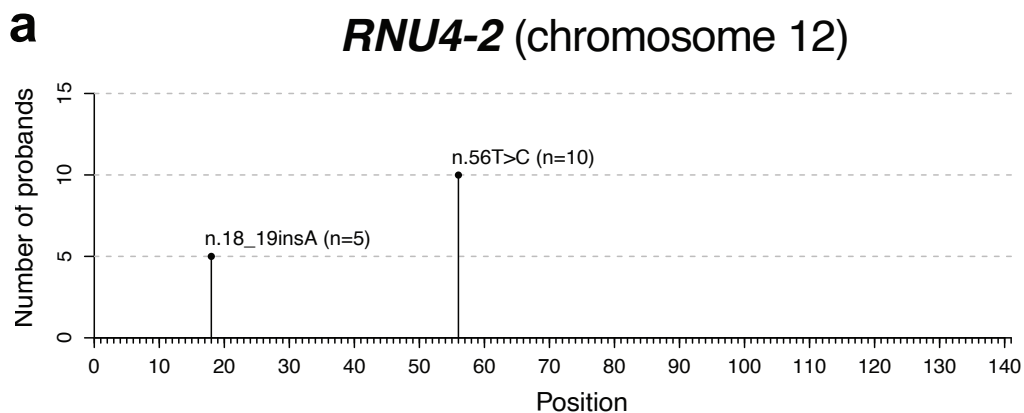
In the format provided by the
authors and unedited



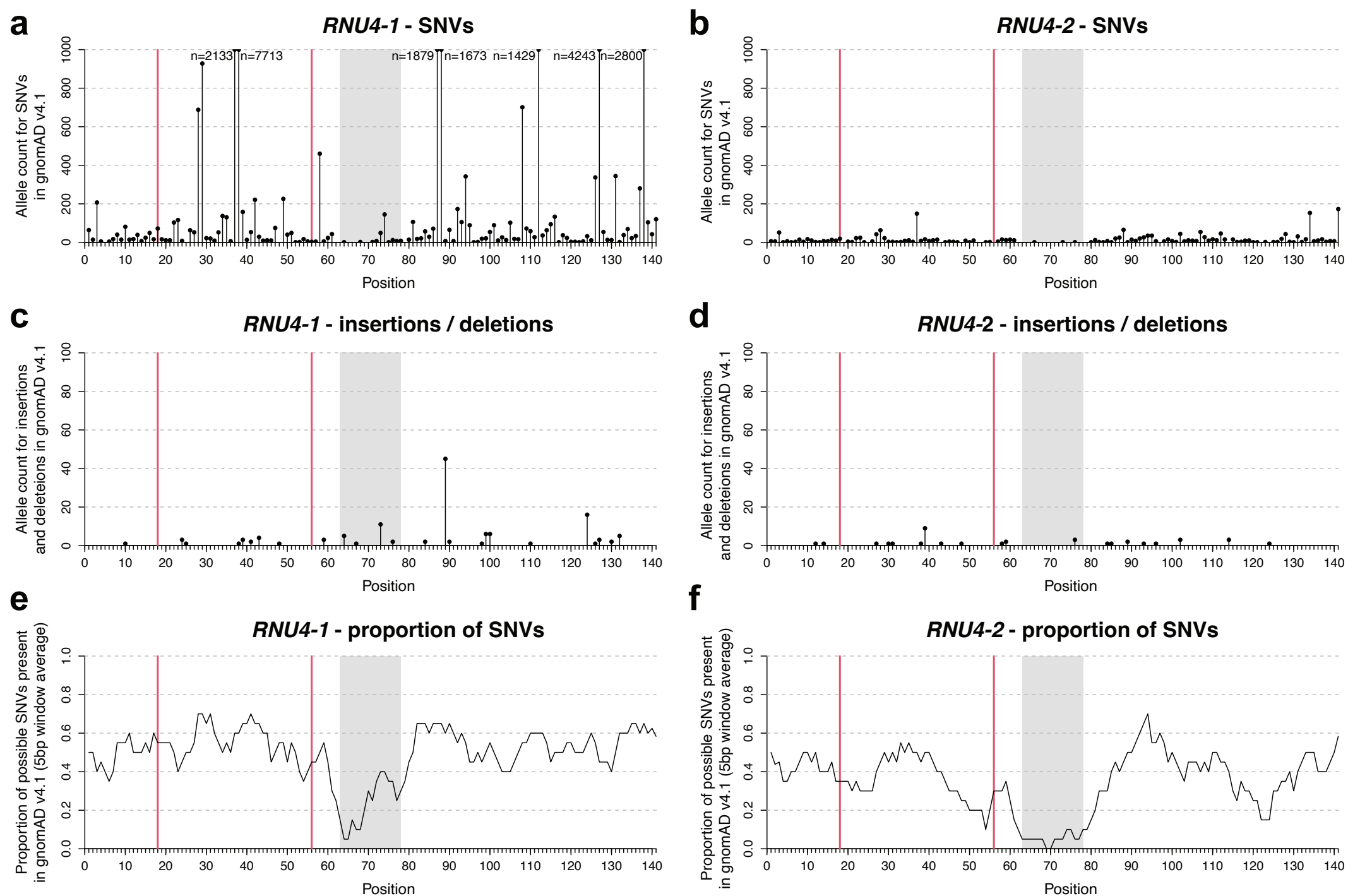
Supplementary Figure 1 | Pedigrees of all patients analyzed. Families are grouped according to their *RNU* genotypes, with affected, carrier, and unaffected individuals indicated by standard pedigree symbols.



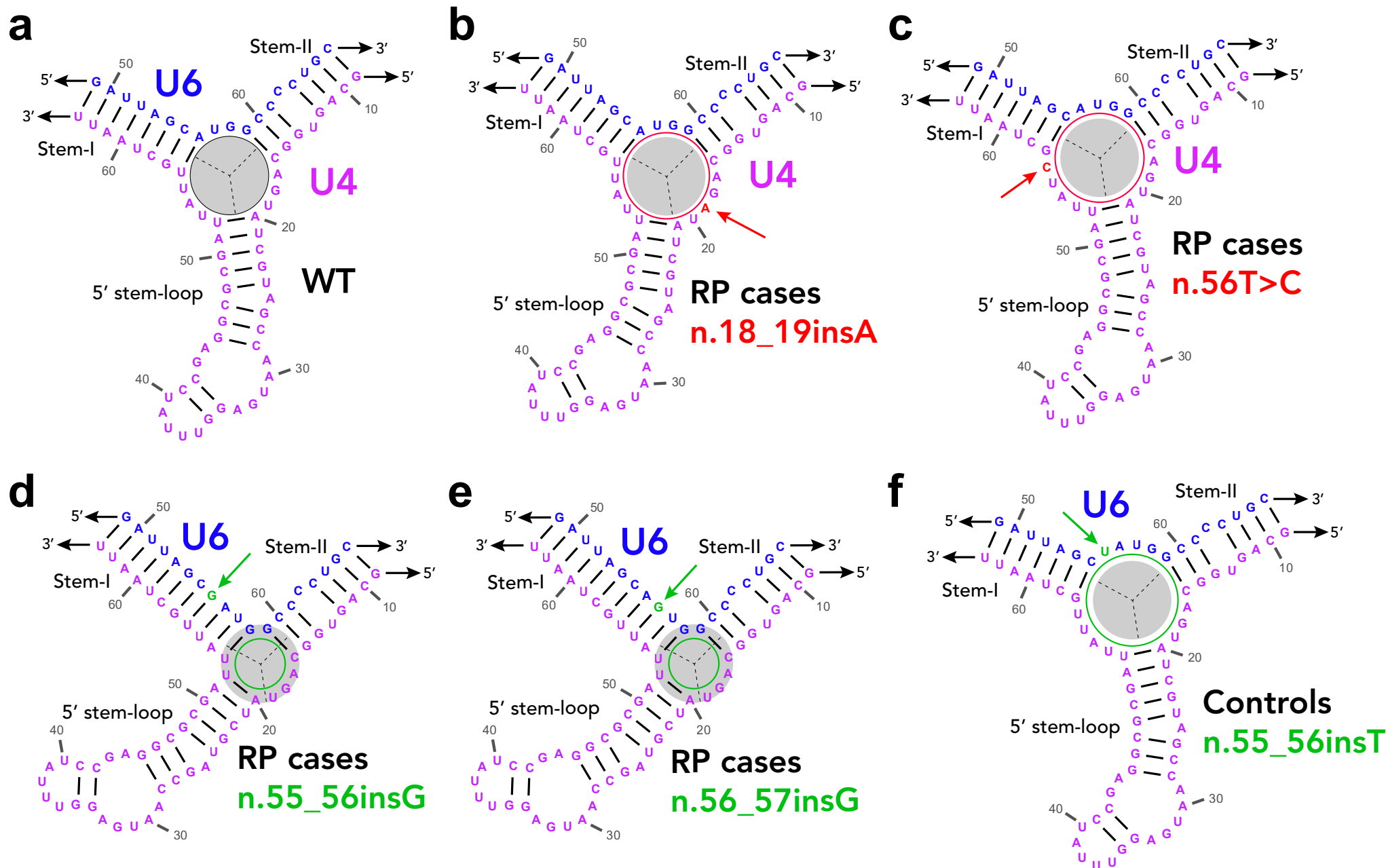
Supplementary Figure 2 | Clinical images of the initial family with adRP and the pathogenic variant n.18_19insA in *RNU4-2* including the father (I:1) and representative affected siblings, I:1, II:1, II:5, II:7 and II:6. a-e, Wide-field and color fundus montage photographs show varying stages of degeneration and bone-spicule pigment deposition (inset) across the midperiphery. Fundus autofluorescence (FAF) showing foveal atrophy **f-g** and the characteristic autofluorescence ring **h-j** delineating area of spared retina. **k-o**, Horizontal spectral-domain optical coherence tomography (SD-OCT) of structurally intact outer retinal layers and the presence of cystoid macular edema **l, n**. **p**, FAF image delineating the contour of the autofluorescent ring (white arrowheads) in II:2. **q**, Contour diagram tracing progressive constriction of the autofluorescent ring over a 4 year period in II:6 (ON, optic nerve; x, fovea). **r**, Thickness profiles of photoreceptor+ on SD-OCT scans across the macula in siblings with visible autofluorescent rings (II:6, II:2, II:3 and II:7) (gray lines) compared to the mean and 95% confidence intervals (CI) (shaded region) of 20 age-matched healthy control eyes. **s**, Normalized photoreceptor+ thicknesses within the autofluorescent ring relative to ± 2 standard deviations (SD) of healthy control eyes.



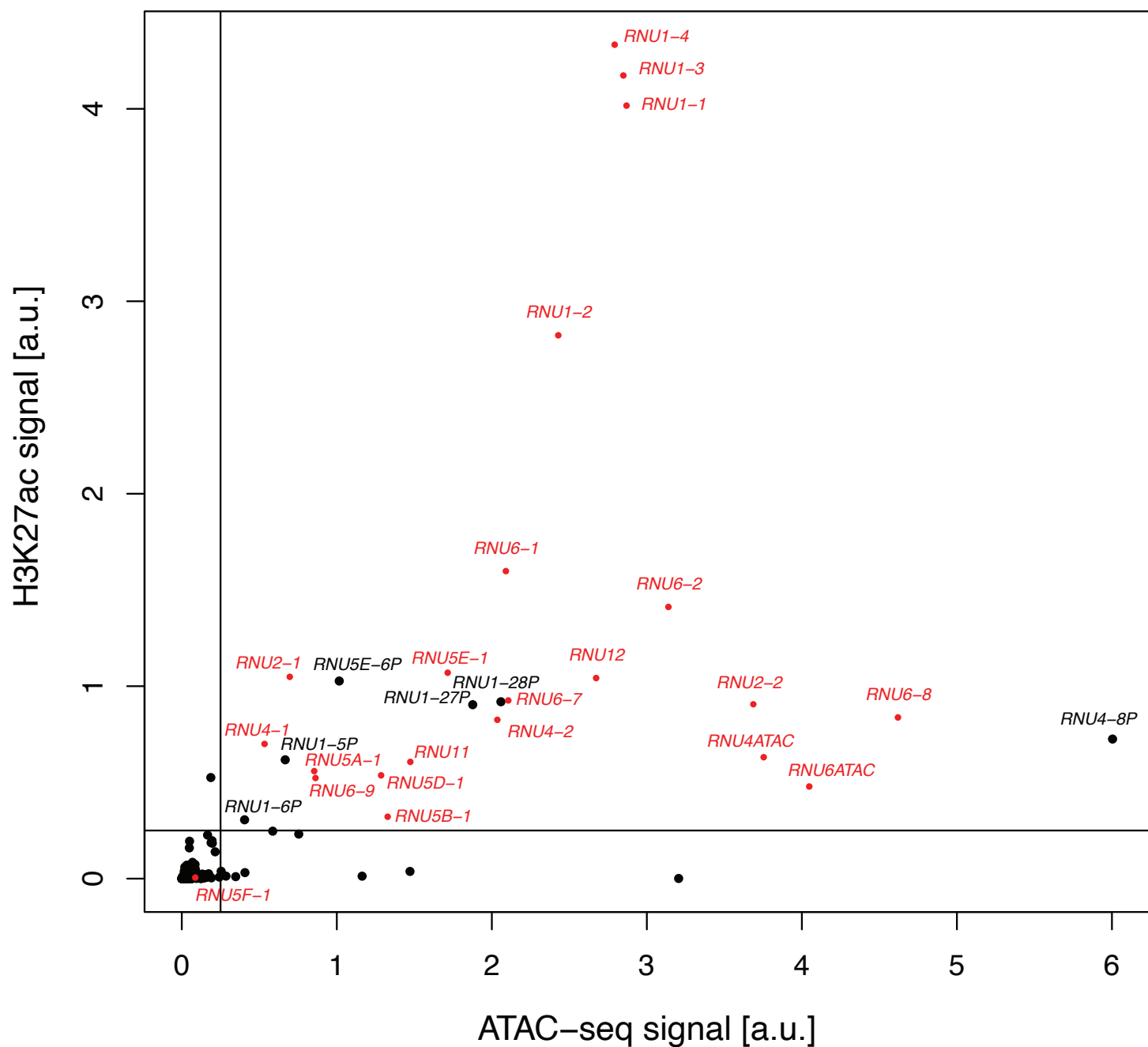
Supplementary Figure 3 | Recurrent pathogenic variants identified in RP cases. **a-e**, Number of probands with pathogenic variants detected in *RNU4-2* (**a**), *RNU6-1* (**b**), *RNU6-2* (**c**), *RNU6-8* (**d**), and *RNU6-9* (**e**). **f**, Cumulative number of probands with pathogenic variants in *RNU6* paralogues.



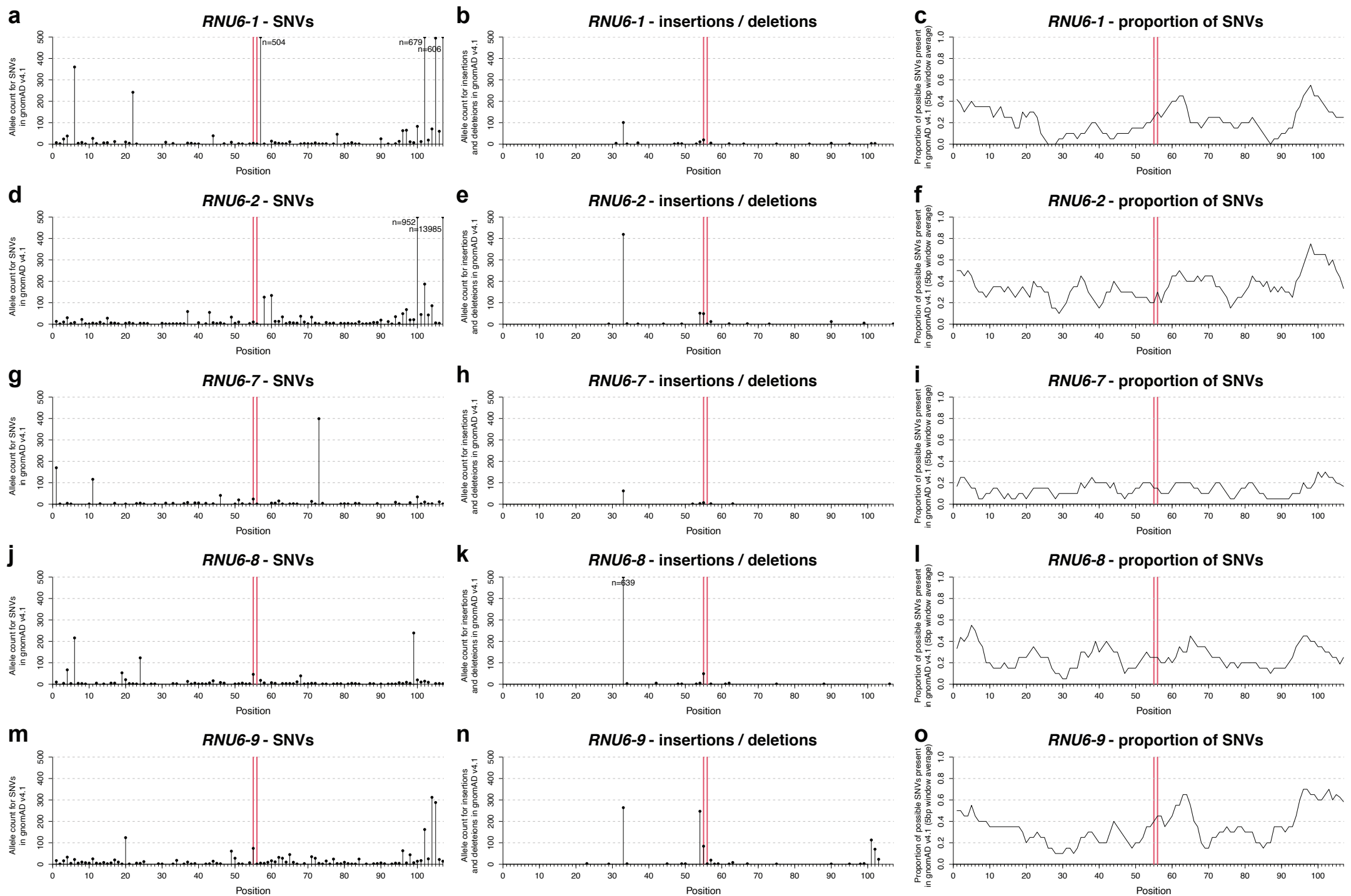
Supplementary Figure 4 | Landscape of variations from gnomAD v4.1 for *RNU4-1* and *RNU4-2*. **a-b**, Allele count of SNVs for *RNU4-1* and *RNU4-2*. **c-d**, Allele count of insertions and deletions for *RNU4-1* and *RNU4-2*. **e-f**, Proportion of possible SNVs for *RNU4-1* and *RNU4-2* with a 5bp running window average. The position of recurrent pathogenic variants causing RP detected in *RNU4-2* are indicated with red lines. The region that contains pathogenic variants in *RNU4-2* causing NDD is shaded in grey.



Supplementary Figure 5 | 2D modeling of the U4-U6 three-way junction. a, Wild-type (WT) structure of the U4/U6 duplex surrounding the internal loop and structures including pathogenic variants affecting U4 (b, c), U6 (d, e), as well as a benign variant in U6 (f). The gray circle gauges the normal size of the three-way junction, while the dashed lines show the normal orientations of the stems originating from the junction.



Supplementary Figure 6 | Markers of transcriptional activity in human retinal tissue in the regions of all *RNU* genes and pseudogenes. Gene (in red) and pseudogene (in black) symbols are indicated when both signals exceed 0.25 arbitrary units (a.u.) (vertical and horizontal black lines).



Supplementary Figure 7 | Landscape of variations from gnomAD v4.1 for *RNU6-1*, *RNU6-2*, *RNU6-7*, *RNU6-8*, and *RNU6-9*. **a, d, g, j, m**, Allele count of SNVs for individual genes. **b, e, h, k, n**, Allele count of insertions and deletions. **c, f, i, l, o**, Proportion of possible SNVs with a 5bp running window average. Vertical red lines show the position of recurrent pathogenic variants underlying RP.

Supplementary Data 1

All affected members of family M1-A experienced a symptomatic onset of night-blindness and progressive loss of peripheral vision beginning in late adolescence to early adulthood. Posterior subcapsular cataracts developed in 5 siblings (II:1-II:5) and I:1 by their 3rd decade. Fundus examination in all affected individuals revealed classical RP features, including waxy disc pallor, attenuated retinal vessels and bone-spicule pigment (BSP) deposition. BSP distribution was most pronounced in the superonasal quadrant, varying in severity from mild specks in the midperiphery to diffuse migration across the posterior pole (Supplementary Fig. 2a-e). Best-corrected visual acuities (BCVA) were stable from 20/20 to 20/60 in siblings, except I:1, whose BCVA declined to hand motion/light perception between the 6th and 7th decades. During the follow up period, I:1, II:1, II:2, II:4 and II:7 developed persistent cystoid macular edema (CME) and further contributed to central vision loss. Fundus autofluorescence (FAF) imaging showed widespread coalescing lesions of RPE atrophy in the periphery with progressive involvement of the fovea in I:1 and II:1 (Supplementary Fig. 2f,g); the spared region of residual function in siblings II:2-II:7 was delineated by a characteristic hyper-autofluorescent “ring” that ranged in size from 5.32 to 50.17 mm² and constricted at a rate of 0.48 to 1.25 mm²/year (Supplementary Fig. 2h-j,p,q) inside the macula. Both RPE and photoreceptor-attributable layers [cone outer segment tips (COST), ellipsoid zone (EZ), external limiting membrane (ELM) and outer nuclear layer (ONL)] were structurally intact within this spared region (Supplementary Fig. 2k-o), although significantly thinned relative to spatially corresponding regions of a healthy retina (Supplementary Fig. 2r,s). In all individuals, dark-adapted (scotopic) 0.01 cd·s/m²

responses were extinguished on full-field electroretinogram (ffERG) testing indicating generalized rod dysfunction. Mixed rod and cone dark-adapted $3.0 \text{ cd} \cdot \text{s/m}^2$ scotopic waveforms were recordable but severely attenuated (b-wave ~17 to 80 μV) in all except 1:1 (extinguished). Light-adapted (photopic) responses were comparatively preserved but nevertheless affected in all cases indicating subsequent cone involvement. 30-Hz flicker peak-to-trough amplitudes ranged from 10 to 50 μV and demonstrated delayed implicit time of >40 ms.